Simulation of quasi-two-dimensional dipolar systems

2003 J. Phys.: Condens. Matter 15 S1471

(http://iopscience.iop.org/0953-8984/15/15/311)

INSTITUTE OF PHYSICS PUBLISHING JOURNAL OF PHYSICS: CONDENSED MATTER

J. Phys.: Condens. Matter **15** (2003) S1471–S1495 PII: S0953-8984(03)55300-0

Simulation of quasi-two-dimensional dipolar systems

J-J Weis

Laboratoire de Physique Théorique, UMR 8627, Université de Paris XI, Bâtiment 210, F-91405, Orsay Cedex, France

Received 28 October 2002
Published 7 April 2003
Online at stacks.iop.org/JPhysCM/15/S1471

Abstract

A brief survey is given of recent simulation work of quasi-two-dimensional (Q2D) systems, monolayers and systems of finite thickness, involving dipolar interactions. Representative examples include colloidal particles at an interface, electrorheological fluids, magnetic thin films, nanocrystals deposited on a substrate etc. Methodological aspects related to the long range of the dipolar interaction and its directional nature (energy calculation, cluster moves) are summarized. Taking as an example a bilayer of dipolar hard spheres, we demonstrate that the energy and structural properties of a thin slab of dipolar particles periodic in two dimensions and finite in the third can be accurately calculated by means of the usual three-dimensional Ewald sum. Some new simulation results for the structural properties of Q2D dipolar hard spheres with additional attraction, in an external field or in bilayers, are presented.

1. Introduction

Dipolar interactions can play a significant role in the structural properties of two-dimensional (2D) systems. They can stabilize long-range order (LRO) in 2D ferromagnets at finite temperature [1–8], entail magnetization switching between in-plane and out-of-plane ordered phases in thin magnetic films [9–12], lead, through competition with attractive short-range interactions, to formation of modulated phases [13], stripes and bubbles, in magnetic thin films [12, 14–16], in thin films of magnet garnets [17, 18], amphiphilic molecules adsorbed at an air–water interface [19–21] etc. They promote self-assembly and formation of crystal superstructures in colloidal nanocrystals [22–25], and determine the rheological properties of suspensions of colloidal particles in an external magnetic or electric field [26], or the orientational structure of polar liquid crystals at an air–water interface [27], to give only a few examples. These phases arise from the interplay of the dipolar interaction with competing interactions like magnetocrystalline anisotropy, exchange interaction, external magnetic or electric field or van der Waals forces.

Computer simulations, Monte Carlo (MC) or molecular dynamics (MD) [28], based on a Hamiltonian of the general form

$$H = \frac{1}{2}\sum_{i\neq j}^{N} v_{sr}(r_{ij}) + \frac{1}{2}g\sum_{i\neq j}^{N}\frac{1}{r_{ij}^{p}}\left[\boldsymbol{s}_i\cdot\boldsymbol{s}_j - \frac{p(\boldsymbol{s}_i\cdot\boldsymbol{r}_{ij})(\boldsymbol{s}_j\cdot\boldsymbol{r}_{ij})}{r_{ij}^{2}}\right] + \tfrac{1}{2}\sum_{i\neq j}^{N} J(r_{ij})\boldsymbol{s}_i\cdot\boldsymbol{s}_j - K\sum_{i}^{N} s_{iz}^{2} - \sum_{i}^{N}\mu\boldsymbol{H}\cdot\boldsymbol{s}_i \qquad (1)$$

have been helpful in elucidating the role of these various interactions in phase behaviour and pattern formation. In equation (1), $v_{sr}(r)$ is an isotropic short-range potential mostly taken to be a hard-sphere potential of diameter σ, a soft-sphere potential $4\epsilon(\sigma/r)^{12}$ or a Lennard-Jones potential $4\epsilon[(\sigma/r)^{12} - (\sigma/r)^{6}]$. The second term is the contribution from the dipole–dipole interaction where $\boldsymbol{s}_i$ and $\boldsymbol{s}_j$ are unit vectors in the direction of the dipole moments of particles i and j, $\boldsymbol{r}_{ij} = \boldsymbol{r}_j - \boldsymbol{r}_i$, the vector joining the centres of mass of the particles, $r_{ij} = |\boldsymbol{r}_{ij}|$ and $g = \mu^2$ (μ dipole moment). The case $p = 3$ (referred to as Q2D), relevant for almost all experimental situations, corresponds to the dipole–dipole interaction in three-dimensional (3D) space, whereas the case $p = 2$ (referred to as 2D), of more theoretical interest, corresponds to the dipolar interaction satisfying 2D electrostatics. In Q2D systems the dipole moments can rotate in full 3D space (unless otherwise stated); they are, obviously, planar in 2D systems.

In continuum simulations the repulsive part (hard or soft sphere) in $v_{sr}(r)$ avoids collapse of the system; in lattice simulations the lattice spacing provides a natural short-range cut-off.

The third term in (1) is the contribution from the short-range exchange interaction, important in continuous or granular magnetic films. In lattice simulations $J(r) = -J$ and its range is limited to nearest neighbours; in continuum models the range of interaction can be restricted to nearest neighbours by a Yukawa potential $J(r) = -J\frac{\mathrm{e}^{-z(r-\sigma)}}{r/\sigma}$ with sufficiently large value of z [29].

The fourth term in equation (1) is the contribution from anisotropy which can have various origins [30] (magnetocrystalline anisotropy caused by the spin–orbit interaction, surface anisotropy due to breaking of the translational symmetry of the magnetic material near a surface etc). For uniaxial systems it can be crudely approximated by a single-site (local) effective anisotropy term of the form given in equation (1) where s_{iz} is the projection of $\boldsymbol{s}_i$ on the easy-axis (z-) direction. Finally, the last term in equation (1) represents the interaction of the dipole moment with an external field $\boldsymbol{H}$.

The aim of the paper is to give a brief survey of recent simulation work on Q2D systems based on equation (1). Although main emphasis will be put on monolayers, a few cases of systems with finite thickness will be considered as well, if the latter is small compared to the other dimensions (few-layer systems, systems confined between electrodes or glass plates, liquid–vapour (L–V) interface etc). For notational convenience we shall refer to these systems as 2D + h.

A distinguishing feature of the dipolar interaction is its slow spatial decay which has to be treated carefully in simulations. Limiting the dipolar interaction to the basic (finite) simulation cell, as is generally done for short-range potentials, would lead to inaccurate results [31]. The most reliable and now widely accepted way to take account of the long-range nature of the dipolar interaction (in fact, for planar systems only the true 2D dipolar potential ($p = 2$), satisfying 2D electrostatics, is strictly long range, in the sense that the energy diverges with system size) is to repeat the simulation cell periodically in space and perform an Ewald sum for the energy [28]. The relevant expressions for the energy will be summarized in section 2 for monolayers (Q2D and 2D) and for slabs (2D+h) where periodicity extends in two directions, the system being finite in the third direction. This section also describes cluster moves designed to

speed up convergence of MC sampling in aggregate forming systems (e.g. strongly interacting Q2D dipolar hard spheres at low density, electrorheological (ER) or magnetorheological (MR) fluids in an external field etc).

We then proceed to give a survey of simulation work (continuum and lattice) starting with the simplest system, dipolar hard spheres, to move to dipolar systems with an additional attraction, in an external field and in competition with anisotropy and exchange interactions.

2. Simulation methods

2.1. Energy

2.1.1. Monolayers. As already stated in the introduction the most appropriate way, presently, to accurately calculate the energy of a system with long-range dipolar interactions is to replicate the basic simulation cell periodically in space and calculate the energy as the sum of the interactions of the N dipoles in the basic cell with all the other dipoles in the cell and with the periodically repeated images in the surrounding cells ($\boldsymbol{\mu}_i = \mu \boldsymbol{s}_i$),

$$U_{dd} = \frac{1}{2}\sum_{i,j=1}^{N}\sum_{\boldsymbol{n}}{}' \left\{ \frac{\boldsymbol{\mu}_i \cdot \boldsymbol{\mu}_j}{|\boldsymbol{r}_{ij} + \boldsymbol{t}\cdot\boldsymbol{n}|^p} - p\frac{[\boldsymbol{\mu}_i \cdot (\boldsymbol{r}_{ij} + \boldsymbol{t}\cdot\boldsymbol{n})][\boldsymbol{\mu}_j \cdot (\boldsymbol{r}_{ij} + \boldsymbol{t}\cdot\boldsymbol{n})]}{|\boldsymbol{r}_{ij} + \boldsymbol{t}\cdot\boldsymbol{n}|^{p+2}} \right\}. \tag{2}$$

For an arbitrary oblique simulation cell, characterized by two basis vectors of lengths L_x and L_y and angle γ, the cell basis matrix $\boldsymbol{t}$ is given by

$$\boldsymbol{t} = \begin{pmatrix} L_x & L_y\cos\gamma \\ 0 & L_y \sin\gamma \end{pmatrix}. \tag{3}$$

The prime in the sum over $\boldsymbol{n} = (n_x, n_y)$, with n_x, n_y integers, means that the term $i \neq j$ is omitted when $\boldsymbol{n} = 0$. For the Q2D system ($p = 3$) the sum (2) is absolutely, but slowly convergent. By a lattice summation technique (Ewald sum) the slowly convergent sum is transformed into two rapidly convergent sums, one in direct space, the other in reciprocal space, the rate of convergence of both sums being regulated by the parameter α. The resulting expression for the energy of the Q2D system is $U_{dd} = U_{\parallel} + U_{\perp}$, where [32]

$$\begin{aligned} U_{\parallel} = -\tfrac{1}{2}\sum_{i,j=1}^{N}\sum_{\boldsymbol{n}}{}' & [B(|\boldsymbol{r}_{ij} + \boldsymbol{t}\cdot\boldsymbol{n}|)\boldsymbol{\mu}_i^{\parallel}\cdot\boldsymbol{\mu}_j^{\parallel} \\ & + C(|\boldsymbol{r}_{ij} + \boldsymbol{t}\cdot\boldsymbol{n}|)[\boldsymbol{\mu}_i \cdot (\boldsymbol{r}_{ij} + \boldsymbol{t}\cdot\boldsymbol{n})][\boldsymbol{\mu}_j \cdot (\boldsymbol{r}_{ij} + \boldsymbol{t}\cdot\boldsymbol{n})]] \\ & + \frac{\pi}{A}\sum_{\boldsymbol{G}\neq 0}\frac{\operatorname{erfc}(G/2\alpha)}{G}F_{\parallel}(\boldsymbol{G})F_{\parallel}^{*}(\boldsymbol{G}) - \frac{2\alpha^3}{3\sqrt{\pi}}\sum_{i=1}^{N}|\boldsymbol{\mu}_i^{\parallel}|^2 \end{aligned} \tag{4}$$

and

$$\begin{aligned} U_{\perp} = -\tfrac{1}{2}\sum_{i,j=1}^{N}\sum_{\boldsymbol{n}}{}' & B(|\boldsymbol{r}_{ij} + \boldsymbol{t}\cdot\boldsymbol{n}|)\mu_i^z\mu_j^z \\ & + \frac{\pi}{A}\sum_{\boldsymbol{G}\neq 0}\left[\frac{2\alpha}{\sqrt{\pi}}\exp\left(-\frac{G^2}{4\alpha^2}\right) - G\operatorname{erfc}\left(\frac{G}{2\alpha}\right)\right]F_{\perp}(\boldsymbol{G})F_{\perp}^{*}(\boldsymbol{G}) \\ & + \frac{2\sqrt{\pi}\alpha}{A}\sum_{i=1}^{N}\sum_{j=1}^{N}\mu_i^z\mu_j^z - \frac{2\alpha^3}{3\sqrt{\pi}}\sum_{i=1}^{N}(\mu_i^z)^2. \end{aligned} \tag{5}$$

In deriving these expressions the dipole moment has been divided into an in-plane component $\boldsymbol{\mu}_i^{\parallel}$ and an out-of-plane component μ_i^z assumed to be along the z-axis. The functions $B(r)$ and

$C(r)$ are given by

$$B(r) = -\frac{\operatorname{erfc}(\alpha r)}{r^3} - \frac{2\alpha}{\sqrt{\pi}}\frac{\exp(-\alpha^2 r^2)}{r^2}, \tag{6}$$

$$C(r) = 3\frac{\operatorname{erfc}(\alpha r)}{r^5} + \frac{2\alpha}{\sqrt{\pi}}\left(\frac{3}{r^2} + 2\alpha^2\right)\frac{\exp(-\alpha^2 r^2)}{r^2}, \tag{7}$$

and

$$F_{\parallel}(\boldsymbol{G}) = \sum_{i=1}^{N}(\boldsymbol{G}\cdot\boldsymbol{\mu}_i^{\parallel})\exp[\mathrm{i}\boldsymbol{G}\cdot\boldsymbol{r}_i], \tag{8}$$

$$F_{\perp}(\boldsymbol{G}) = \sum_{i=1}^{N}\mu_i^z \exp[\mathrm{i}\boldsymbol{G}\cdot\boldsymbol{r}_i]. \tag{9}$$

In equations (4) and (5), $A = L_x L_y \sin\gamma$ is the area of the simulation cell, N the number of particles, erfc denotes the complementary error function and F^* the complex conjugate of F. The wavevectors $\boldsymbol{G}$ which enter the reciprocal space contributions to the energy are of the form

$$\boldsymbol{G} = 2\pi({}^t\boldsymbol{t})^{-1}\boldsymbol{n}, \tag{10}$$

where ${}^t\boldsymbol{t}$ denotes the transpose of $\boldsymbol{t}$, with components

$$G_x = \frac{2\pi}{A}L_x \sin\gamma n_x \tag{11}$$

$$G_y = \frac{2\pi}{A}(-L_y\cos\gamma n_x + L_x n_y) \tag{12}$$

and modulus

$$G = \sqrt{G_x^2 + G_y^2}. \tag{13}$$

Care has to be taken to properly choose the α parameter which governs the rate of convergence of the real- and reciprocal-space contributions in equations (4) and (5). It is generally taken sufficiently large that only the terms with $\boldsymbol{n} = 0$ need to be retained in equations (4) and (5).

Although no simulation work will be reported in this review for the true 2D dipolar system, it seems, nevertheless, instructive to contrast the corresponding Ewald sums with those of the Q2D system. The main difference lies in the fact that for 2D systems the sum in equation (2) is only conditionally convergent and will depend on the way the summation is performed. By summing over circular shells one has (EW2D) [33, 36]

$$\begin{aligned} U_{dd} = -\tfrac{1}{2}\sum_{i,j=1}^{N}{\sum_{\boldsymbol{n}}}'[&b(|\boldsymbol{r}_{ij}+\boldsymbol{t}\cdot\boldsymbol{n}|)\boldsymbol{\mu}_i\cdot\boldsymbol{\mu}_j \\ &+ c(|\boldsymbol{r}_{ij}+\boldsymbol{t}\cdot\boldsymbol{n}|)[\boldsymbol{\mu}_i\cdot(\boldsymbol{r}_{ij}+\boldsymbol{t}\cdot\boldsymbol{n})][\boldsymbol{\mu}_j\cdot(\boldsymbol{r}_{ij}+\boldsymbol{t}\cdot\boldsymbol{n})]] \\ &+ \frac{\pi}{A}\sum_{G\neq 0}\frac{\exp(-G^2/4\alpha^2)}{G^2}F(\boldsymbol{G})F^*(\boldsymbol{G}) \\ &- \frac{1}{2}\alpha^2\sum_{i=1}^{N}\boldsymbol{\mu}_i^2 + \frac{\pi}{2A}\left(1-\frac{\epsilon'-1}{\epsilon'+1}\right)\left(\sum_{i=1}^{N}\boldsymbol{\mu}_i\right)^2 \end{aligned} \tag{14}$$

where the functions $b(r)$ and $c(r)$ are given by

$$b(r) = -\frac{\exp(-\alpha^2 r^2)}{r^2}, \tag{15}$$

$$c(r) = 2\left(\frac{1}{r^2}+\alpha^2\right)\frac{\exp(-\alpha^2 r^2)}{r^2}, \tag{16}$$

and

$$F(\boldsymbol{G}) = \sum_{i=1}^{N} (\boldsymbol{G} \cdot \boldsymbol{\mu}_i) \exp[\mathrm{i}\boldsymbol{G} \cdot \boldsymbol{r}_i]. \tag{17}$$

The last term in equation (14), which has no equivalent in the Q2D case, represents the contribution to the energy from the depolarization field created when a continuous medium of dielectric constant ϵ' surrounds a disc-shaped sample of periodic replica. For a conducting medium ($\epsilon' = \infty$) this term vanishes while for a system in vacuum ($\epsilon' = 1$) it is $\frac{\pi}{2A}\boldsymbol{M}^2$, where $\boldsymbol{M}$ is the total polarization of the system. This (positive) term makes ferroelectric behaviour energetically unfavourable and is at the origin (as shown in 3D dipolar soft-and hard-sphere simulations [34, 35]) of domain formation, thereby lowering the polarization and thus the energy.

An alternative method to simulate Q2D or 2D dipolar systems, which avoids use of periodic boundary conditions, is to place the centres of the particles on the surface of a sphere in 3D space (hypersphere geometry) [37]. This method, which is computationally faster than the Ewald method, has so far been applied only to the true 2D dipolar potential [38]. In this geometry the dipole potential is taken to be the solution of Poisson's equation on a sphere.

2.1.2. Slab geometry $2D+h$. In simulations of systems with slab geometry (polar molecules at interfaces, colloids confined between plates etc), the system is generally considered periodic in two dimensions (say x and y) and is finite in the third direction. In this geometry an Ewald sum (EW2D + h) is still possible [39–42] but, due to the lack of periodicity in one direction, the corresponding expressions for the energy turn out to be more complicated than for the Q2D (or 3D and 2D) cases. Splitting coordinates $\boldsymbol{r}_{ij}(\boldsymbol{\varrho}_{ij}, z_{ij})$ and dipole moments $\boldsymbol{\mu}_i(\boldsymbol{\mu}_i^{\parallel}, u_i^z)$ into components parallel and perpendicular to the slab surfaces, one has [42] ($U_{dd} = U_{\parallel} + U_{\perp}$)

$$\begin{aligned} U_{\parallel} = -\tfrac{1}{2} \sum_{i,j=1}^{N} {\sum_{\boldsymbol{n}}}' & [B(|\boldsymbol{\varrho}_{ij} + \boldsymbol{t}\cdot\boldsymbol{n}, z_{ij}|)\boldsymbol{\mu}_i^{\parallel} \cdot \boldsymbol{\mu}_j^{\parallel} \\ & + C(|\boldsymbol{\varrho}_{ij} + \boldsymbol{t}\cdot\boldsymbol{n}, z_{ij}|)[\boldsymbol{\mu}_i \cdot (\boldsymbol{\varrho}_{ij} + \boldsymbol{t}\cdot\boldsymbol{n}, z_{ij})][\boldsymbol{\mu}_j \cdot (\boldsymbol{\varrho}_{ij} + \boldsymbol{t}\cdot\boldsymbol{n}, z_{ij})]] \\ & + \frac{\pi}{2A} \sum_{i,j=1}^{N} \sum_{G\neq 0} \frac{1}{G}[D(G, z_{ij}) + D(G, -z_{ij})](\boldsymbol{\mu}_j^{\parallel} \cdot \boldsymbol{G})(\boldsymbol{\mu}_i^{\parallel} \cdot \boldsymbol{G})\mathrm{e}^{\mathrm{i}\boldsymbol{G}\cdot\boldsymbol{\varrho}_{ij}} \\ & - \frac{2\alpha^3}{3\sqrt{\pi}} \sum_{i=1}^{N} |\boldsymbol{\mu}_i^{\parallel}|^2, \end{aligned} \tag{18}$$

and

$$\begin{aligned} U_{\perp} = -\tfrac{1}{2} \sum_{i,j=1}^{N} {\sum_{\boldsymbol{n}}}' & B(|(\boldsymbol{\varrho}_{ij} + \boldsymbol{t}\cdot\boldsymbol{n}, z_{ij})|)\mu_i^z \mu_j^z \\ & + \frac{\pi}{2A} \sum_{i,j=1}^{N} \sum_{G\neq 0} \{E(G, z_{ij}) - G[D(G, z_{ij}) + D(G, -z_{ij})]\}\mu_i^z \mu_j^z \mathrm{e}^{\mathrm{i}\boldsymbol{G}\cdot\boldsymbol{\varrho}_{ij}} \\ & + \frac{\pi}{2A} \sum_{i,j=1}^{N} \frac{4\alpha}{\sqrt{\pi}} \mathrm{e}^{-\alpha^2 z_{ij}^2} \mu_i^z \mu_j^z \\ & + \frac{\pi}{2A} \sum_{i,j=1}^{N} \sum_{G\neq 0} (-\mathrm{i})[D(G, z_{ij}) - D(G, -z_{ij})][\mu_i^z (\boldsymbol{\mu}_j^{\parallel} \cdot \boldsymbol{G}) + \mu_j^z (\boldsymbol{\mu}_i^{\parallel} \cdot \boldsymbol{G})]\mathrm{e}^{\mathrm{i}\boldsymbol{G}\cdot\boldsymbol{\varrho}_{ij}} \end{aligned}$$

$$-\frac{2\alpha^3}{3\sqrt{\pi}}\sum_{i=1}^{N}(\mu_i^z)^2, \tag{19}$$

where the functions B and C are defined in equtions (6) and (7), repectively, and

$$E(G,z)=\frac{4\alpha}{\sqrt{\pi}}\exp\left(-\frac{G^2}{4\alpha^2}-\alpha^2z^2\right) \tag{20}$$

$$D(G,z)=\mathrm{e}^{Gz}\mathrm{erfc}\left(\frac{G}{2\alpha}+\alpha z\right). \tag{21}$$

A shortcoming of expressions (18) and (19) is that the double sum in i and j, due to the complicated way the bounded coordinates enter the expressions, cannot be reduced, as for Q2D or 2D, to a sum of order N. This makes the method rather impractical for use. Several methods have been proposed to bypass this drawback.

(i) The expressions (18) and (19) for the energy are retained but pair interactions are calculated in advance for a large number of dipole–dipole configurations and tabulated in convenient form. Interactions of dipoles in the basic simulation cell are calculated exactly [43].

(ii) The slab is placed at the centre of a parallelepipedic simulation box which has dimension perpendicular to the slab much larger than the width of the latter and a 3D Ewald sum is applied [31, 44, 45]. In this way one effectively simulates an infinite number of parallel slabs. For a sufficiently large empty space separating the slabs one expects the influence of the periodic images on the behaviour of the system to become negligible. If the total dipole moment of the slab in the perpendicular direction $M_z=\sum\mu_i^z$ is non-zero, contributions from image cells in the z-direction can be eliminated by supplementing the usual 3D Ewald sum (with conducting boundary conditions) [28, 46] with a correction term $2\pi M_z^2/A$ [45, 47–49]. This procedure will be referred to as EW3DC.

(iii) The dipole interaction is expanded in powers in z_{ij}/ϱ_{ij} and an Ewald sum applied to the in-plane component of the interaction. This method, proposed by Hautman and Klein [50], should be appropriate for narrow slabs.

(iv) Use of a hyperspherical geometry. The dipolar particles are confined between two surfaces, separated by a distance h, located symmetrically with respect to the equator of a hypersphere $\mathcal{S}_3$ in 4D Euclidean space. This geometry has been applied so far only to Coulomb systems [51–53].

(v) A different summation method, as proposed by Lekner [54, 55], is used.

(vi) A novel method, called MMM2D, proposed by Arnold and Holm [56] whose time demand scales as $\mathcal{O}(N^{5/3})$, may prove an efficient alternative when adapted to point dipoles.

A systematic comparison of these different methods for simple point dipolar systems is still lacking. Mecke *et al* have compared (i) and (ii) and found good agreement for the orientational structure in the L–V interface of a Stockmayer (Lennard-Jones + dipole–dipole interaction) system. Here we make further comparison between the EW2D + h and EW3DC methods for a system of dipolar hard spheres with centres of mass constrained to move in two parallel planes (L_1 and L_2) separated by a distance h (bilayer). Due to the fact that, in this case, all pair distances z_{ij} normal to the layers are constant ($=h$), the reciprocal space contributions (18) and (19) can again be cast in a form having similar computational efficiency as in the monolayer case:

$$U_{\parallel}=-\tfrac{1}{2}\sum_{i,j=1}^{N}\sum_{\boldsymbol{n}}{}'[B(|\boldsymbol{\varrho}_{ij}+\boldsymbol{t}\cdot\boldsymbol{n},z_{ij}|)\boldsymbol{\mu}_i^{\parallel}\cdot\boldsymbol{\mu}_j^{\parallel} + C(|\boldsymbol{\varrho}_{ij}+\boldsymbol{t}\cdot\boldsymbol{n},z_{ij}|)[\boldsymbol{\mu}_i\cdot(\boldsymbol{\varrho}_{ij}+\boldsymbol{t}\cdot\boldsymbol{n},z_{ij})][\boldsymbol{\mu}_j\cdot(\boldsymbol{\varrho}_{ij}+\boldsymbol{t}\cdot\boldsymbol{n},z_{ij})]]$$

$$+\frac{\pi}{A}\sum_{G\neq 0}\frac{\operatorname{erfc}(G/2\alpha)}{G}[F_{\parallel}^{(1)}(\boldsymbol{G})F_{\parallel}^{*(1)}(\boldsymbol{G})+F_{\parallel}^{(2)}(\boldsymbol{G})F_{\parallel}^{*(2)}(\boldsymbol{G})]$$
$$+\frac{\pi}{A}\sum_{G\neq 0}\frac{1}{G}[D(G,h)+D(G,-h)]\operatorname{Re}[F_{\parallel}^{(1)}(\boldsymbol{G})F_{\parallel}^{*(2)}(\boldsymbol{G})]$$
$$-\frac{2\alpha^3}{3\sqrt{\pi}}\sum_{i=1}^{N}|\boldsymbol{\mu}_i^{\parallel}|^2 \tag{22}$$

and

$$U_{\perp}=-\tfrac{1}{2}\sum_{i,j=1}^{N}{\sum_{\boldsymbol{n}}}'B(|(\boldsymbol{\varrho}_{ij}+\boldsymbol{t}\cdot\boldsymbol{n},z_{ij})|)\mu_i^z\mu_j^z$$
$$+\frac{\pi}{A}\sum_{G\neq 0}\left[\frac{2\alpha}{\sqrt{\pi}}\exp\left(-\frac{G^2}{4\alpha^2}\right)-G\operatorname{erfc}\left(\frac{G}{2\alpha}\right)\right][F_{\perp}^{(1)}(\boldsymbol{G})F_{\perp}^{*(1)}(\boldsymbol{G})$$
$$+F_{\perp}^{(2)}(\boldsymbol{G})F_{\perp}^{*(2)}(\boldsymbol{G})]$$
$$+\frac{\pi}{A}\sum_{G\neq 0}\{E(G,h)-G[D(G,h)+D(G,-h)]\}\operatorname{Re}[F_{\perp}^{(1)}(\boldsymbol{G})F_{\perp}^{*(2)}(\boldsymbol{G})]$$
$$+\frac{\pi}{2A}\frac{4\alpha}{\sqrt{\pi}}\mathrm{e}^{-\alpha^2h^2}\left(\sum_i\mu_i^z\right)^2$$
$$+\frac{\pi}{A}\sum_{G\neq 0}[D(G,h)-D(G,-h)]\operatorname{Im}[F_{\perp}^{(1)}(\boldsymbol{G})F_{\parallel}^{*(2)}(\boldsymbol{G})+F_{\parallel}^{(1)}(\boldsymbol{G})F_{\perp}^{*(2)}(\boldsymbol{G})]$$
$$-\frac{2\alpha^3}{3\sqrt{\pi}}\sum_{i=1}^{N}(\mu_i^z)^2 \tag{23}$$

with

$$F_{\parallel}^{(1,2)}(\boldsymbol{G})=\sum_{i\in L_1(L_2)}(\boldsymbol{G}\cdot\boldsymbol{\mu}_i^{\parallel})\exp[\mathrm{i}\boldsymbol{G}\cdot\boldsymbol{\varrho}_i], \tag{24}$$
$$F_{\perp}^{(1,2)}(\boldsymbol{G})=\sum_{i\in L_1(L_2)}\mu_i^z\exp[\mathrm{i}\boldsymbol{G}\cdot\boldsymbol{\varrho}_i]. \tag{25}$$

In table 1 we compare the energies obtained with the EW2D + h and EW3DC methods for different layer separations, reduced dipole moments $\mu^*=(\mu^2/\sigma^3kT)^{1/2}$ and densities $\rho^*=N\sigma^2/A$ (N is the number of particles in each layer, A the area of the layer, k the Boltzmann constant and T the temperature). They agree within statistical error for all states considered. For lower temperatures (higher dipole moments) the comparison may be less conclusive as convergence is slow and the system easily trapped in metastable states, probably different in the two methods. Good agreement is also obtained for the pair correlation functions, as illustrated for one thermodynamic state in figure 1.

In simulations where the dielectric constant or permittivity of the medium inside the slab is different from that of the outside medium care has to be taken that the boundary conditions for the electric or magnetic field at the layer surfaces are properly dealt with (for instance in ER fluids near conducting electrodes, inverse ferrofluids (magnetic holes), phospholipid bilayers etc). This is most conveniently accomplished using the method of images [57–62]. A particular favourable case is that of dipoles interacting with metal walls (or any conductive medium). The dipoles and their images then form a periodic 3D array in which the unit cell consists of the original cell enclosing the system and a first image of the dipoles in the fundamental

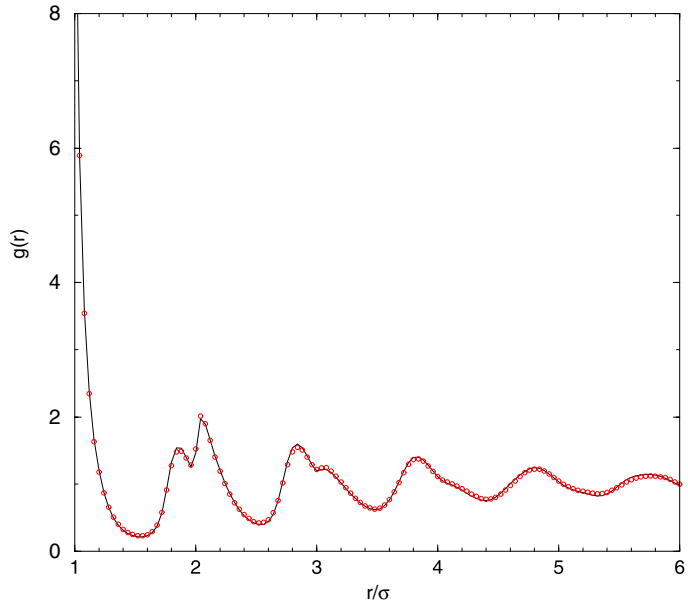

Figure 1. Comparison of the intralayer pair distribution functions $g(r)$ in a bilayer of Q2D dipolar hard spheres obtained from MC simulations using EW2D + h and EW3DC methods. The layer separation is $h = 1.2\sigma$, the density in each layer $\rho^* = 0.92$ and the dipole moment $\mu^* = 2$. The box lengths are in units of σ.

(This figure is in colour only in the electronic version)

Table 1. Energies $U/2NkT$ of a bilayer of dipolar hard spheres using EW2D + h and EW3DC methods. h is the distance between the two layers, ρ^* the layer density and μ^* the reduced dipole moment. The number of particles in each layer is 576. The error on the energy is typically ± 0.02. The dipole moments rotate in full 3D space except for the states marked with an asterisk where they rotate in the layers.

h	ρ^*	μ^*	EW2D + h	EW3DC
0.2	0.45	1.5	−3.13	−3.13
1.05	0.8	2.75	−15.65	−15.61
1.05	0.8	1.5	−2.92	−2.96
1.05*	0.8	1.5	−3.58	−3.56
1.20	0.92	2.0	−7.64	−7.64
1.20	0.6	1.0	−0.51	−0.55
1.20*	0.6	1.0	−0.82	−0.82

cell. The energy of the system can thus be evaluated by performing a 3D Ewald sum on this periodically repeated doubled cell [63, 64].

The computational cost of Ewald sums, which increases with particle number as $\mathcal{O}(N^2)$ or at best $\mathcal{O}(N^{3/2})$ through optimized implementation of the method [65], is acceptable only up to a few thousand particles. If larger systems need to be considered (macromolecules, formation of thick domains in magnetic films, see below), particle mesh Ewald (PME) or fast multipole methods (FMM) will be more efficient alternatives (for a review see [66]). The PME approach [67–69] is similar in spirit to the Ewald method except that the complex exponentials in $F(\boldsymbol{G})$ (cf equations (8), (9)) are replaced by appropriate linear combinations of their values

at nearby grid points (using e.g. B-spline function interpolation). The trigonometric sums can then be evaluated by the computationally efficient fast Fourier transforms (FFT) thereby reducing the complexity of the reciprocal space terms to order $\mathcal{O}(N \ln N)$.

FMM [70] or cell multipole moment methods [71] follow a different strategy, taking advantage of the slow spatial variation of the far part of the particle interactions. In this approach the simulation cell is divided into a tree of progressively smaller subcells. Interactions within a subcell and between the subcell and the nearest-neighbour subcells are calculated exactly while those involving subcells of more distant particles are evaluated by a multipole expansion. Both the FMM [72] and PME [73] methods have been adapted to 3D dipolar systems; for the Q2D case a formulation has been given by Stoycheva and Singer [74] in their study of stripe melting in magnetic monolayers (see below). PME methods have also been developed for 2D + h Coulomb systems [75] but have not yet been adapted to point dipolar systems.

2.2. Cluster moves

As shown below, low-density, low-temperature dipolar hard spheres or dipolar particles in a strong external field form aggregates (chains or rings) in which the particles are strongly bound. MC trial moves that pull particles apart are thus likely to be rejected unless extremely small translational and rotational steps are used. To speed up sampling of configuration space one can combine single-particle moves with cluster moves where a cluster is translated and/or rotated as a whole. Use of a cluster algorithm requires a rule which defines the cluster, e.g. two particles i and j belong to a cluster with probability $p(i, j)$ and are disconnected with probability $1 - p(i, j)$ [46, 76]. For a large class of $p(i, j)$ a general expression for the ratio of acceptance probabilities has been derived in [46, 76]. It is particularly simple when a proximity criterion is used to define a cluster, namely $p(i, j) = 1$ if the distance between two particles $r_{ij} < r_c$, and $p(i, j) = 0$ otherwise [76–78]. Detailed balance then requires that a trial cluster move is rejected (other than on energy grounds) if the connectivity of the cluster changes.

A different method for identifying clusters is proposed in [79]: among all possible partitionings of N dipolar particles into clusters an optimum one is selected which maximizes the entropy under the constraint of minimizing the dipolar energy. Cluster algorithms have been implemented in simulations of strongly interacting low-density Q2D dipolar hard spheres [80, 81] and in Q2D dipolar hard spheres in an external field [78].

3. Dipolar hard spheres

In this section we consider the simplest system with dipolar interactions, namely Q2D dipolar hard spheres (hard spheres with a point dipole moment at the centre). It can be considered as a crude model for providing clues to the understanding of a variety of experimental situations including monolayers of amphiphile molecules adsorbed at a water/air interface [82–86], colloidal spheres dispersed in a ferrofluid [87], magnetic microspheres floating on a liquid surface [88] or a meniscus [89], magnetic or dielectric particles confined between glass plates [90] or on a water/air interface [91], smectic phases of molecules with transverse dipoles [92] etc.

The ground state of an infinite Q2D system of (in-plane) dipoles depends on the lattice structure. For a lattice with rhombicity angle γ it is ferromagnetic for $\gamma < 80°$ and antiferromagnetic for $80° < \gamma \leqslant 90°$ [93]. It is continuously degenerate at $\gamma = 60°$ (triangular lattice) and 90° (square lattice). For the square planar system the lowest-energy configuration corresponds to a vortex arrangement where the dipole moments on the four vertices of a (square) plaquette make angles α, $-\alpha$, $\pi + \alpha$ and α, respectively with the x-axis [94]. The energy is

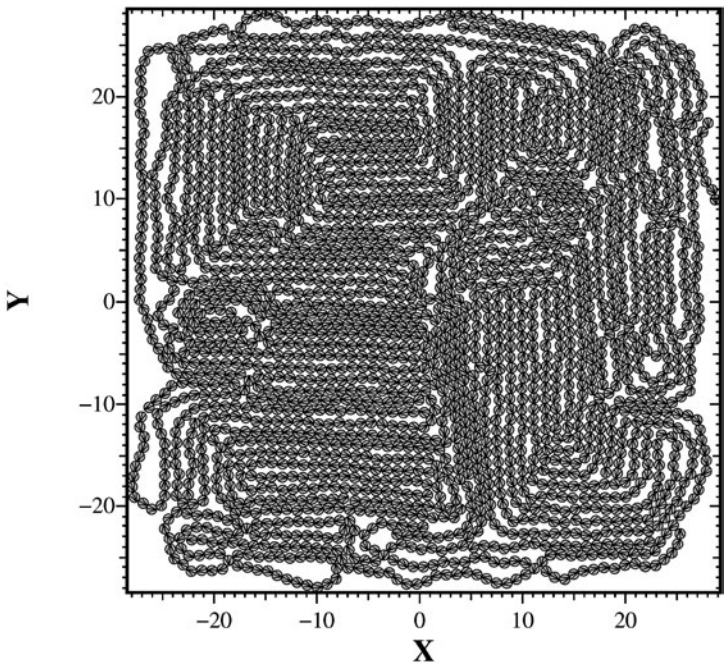

Figure 2. Snapshot of a configuration of 2500 Q2D dipolar hard spheres with free boundaries after 500 000 MC trial moves per particle. The density is $\rho^* = 0.99$ and the dipole moment $\mu^* = 3$. The system is started from a square lattice with random orientations of the dipole moments. Arrows represent the projections of the dipole moments on the xy-plane. Dimensions along the x- and y-axes are in units of σ.

independent of α. Thermal fluctuations can lift the degeneracy of the ground state [5, 95, 96] and select a value of α compatible with the symmetry of the underlying lattice, e.g., $\alpha = 0$ (antiferroelectrically ordered columns of dipoles along the y-axis) or $\pi/4$, for the square lattice. In finite systems the ground state is no longer continuously degenerate. For instance, in the ground state of a finite 22×22 square lattice of dipoles the dipoles align antiferroelectrically along the edges but adopt a microvortex structure ($\alpha = \pi/4$) in the centre of the sample [97]. Formation of vortices is also apparent in low-temperature configurations of dipoles on a disc-shaped lattice with free boundaries [98].

The orientational structure at finite temperature is less well documented. MC simulations of a continuum system of dipolar hard spheres at $\mu^* = 3$ (or reduced temperature $T^* = 1/\mu^{*2} = 1/9$) in the solid phase show formation of faceted domains with edges along the simulation cell axes. For a hexagonal (triangular) lattice the domains have hexagonal shape and within them the dipoles orient in a vortex-like structure [29]. In contrast, on a square lattice more or less rectangular domains seem favoured, within which the dipoles organize into rows parallel to the axes of the simulation cell [99]. A snapshot of a configuration of dipolar hard spheres on a square lattice with free boundary is shown in figure 2. It should be stressed, however, that, at dipole moments larger than about 2.75 ($T^* < 0.13$), the system can be trapped for long times in local energy minima and a true equilibrium not be reached in simulations of reasonable length.

The melting mechanism of in-plane Q2D dipolar hard spheres has, to the best of my knowledge, not been investigated in detail. Below melting, due to the highly directional nature

of the dipolar interaction, the dipolar hard spheres form large linear structures percolating through the simulation cell with a strong tendency for loop formation [29, 99]. Only at densities ρ^* lower than about 0.15 (at $\mu^* = 2.75$–3) do the dipolar spheres self-assemble into aggregates of different sizes, linear chains, rings or more complex clusters, called defect structures, exhibiting different number of branches (mostly three and four) [81, 86, 99, 100]. These clusters evolve by breaking and recombining, the relative concentration of chains, rings and defect clusters and their sizes depending on density and temperature. Quite remarkably, similar structures have been observed in 2D experiments of magnetic microspheres dispersed on a silicon wafer [101], self-assembly of Co nanocrystals [25] and ferrofluids [102]. A quantitative analysis of the conformational properties and length distributions of the simulated dipolar chains and rings suggests [81, 99] that the structure of the Q2D dipolar fluid is the same as that of 2D equilibrium polymers [103–105]. In particular, it is shown that the radius of gyration $R_g \sim n^{\nu}$ scales with exponent $\nu = 3/4$ for chains of length n larger than 10σ and for rings of length larger than 40σ in the density range $0.025 < \rho^* < 0.05$ and for dipole moments $\mu^* = 2.5$–3. For much larger dipole moments, when particles aggregate irreversibly, the fractal dimension $D_f = 1/\nu$ of 2D aggregate has been determined by experiment [106–108] and by lattice [109] and off-lattice simulations [106, 108, 110, 111] based on particle–cluster or cluster–cluster aggregation models. The fractal dimension is shown to shrink with dipole moment reaching a value of approximately 1.2 when $\mu^* \to \infty$.

A still open question is whether Q2D, 2D (and also 3D [112]) dipolar hard spheres can undergo an L–V or some other kind of transition at low density, for instance a topological transition [113–115] or a Bose–Einstein type condensation [116, 117]. The extensive MC simulations of Tavares *et al* [81] for Q2D in-plane dipolar hard spheres at low density did not give any indication of a L–V transition. Similar to the 3D case [118, 119] a minimum amount of dispersive attraction seems necessary to drive condensation [32]. To investigate this question further we performed MC with an attractive Yukawa potential $v_{att}(r) = -\epsilon \frac{e^{-z(r-\sigma)}}{r/\sigma} (\epsilon > 0)$, progressively added to the dipole potential. Snapshots of configurations are shown in figures 3–6 for $\rho^* = 0.2$ and 0.35. At dipole moment $\mu^* = 2.75$ and density $\rho^* = 0.2$ the dipolar hard spheres form, in the absence of the attractive potential, winding, more or less linear structures, spanning the simulation cell (figure 3). The effect of the attractive potential is to form a much more rigid network within which links appear to be made of several rows of dipolar spheres (see figure 4). The situation is different at the lower dipole moment $\mu^* = 1.5$. By turning on the attractive Yukawa potential, the particles, initially in a nearly isotropic state, collapse into compact globules (figure 5) which eventually aggregate into one big drop, typical of two-phase coexistence. Quite strikingly, the particle arrangement shown in figure 6 for $\rho^* = 0.35$, $\mu^* = 2.24$ and $\epsilon/kT = 2.25$ is not without resemblance to the particle organization observed in 15.5 nm magnetic nanoparticles deposited on a water subphase [120].

In contrast to the 3D case [34, 35], no ferroelectric ordering seems to occur in Q2D dipolar hard spheres at liquid densities, although lattice simulations have shown that in-plane dipoles on a square lattice can order ferromagnetically below a non-zero critical temperature [5]. Interestingly, MC simulations [121] of soft dipolar hard spheres confined between two planar non-conducting walls show that, in conditions where the bulk system is ferroelectric [34], LRO persists down to wall separations $h = 7\sigma$ and occurs at pressures lower than in the bulk.

Bilayers of dipolar hard spheres can serve as crude models to investigate the coupling between layers in magnetic films [122] or the structure of polar headgroups in phospholipid bilayers [123]. Snapshots of configurations of dipolar hard spheres with dipole moment $\mu^* = 2.75$ in a bilayer with layer separation $h = 0.5\sigma$ are shown in figures 7 and 8 for layer densities $\rho^* = 0.15$ and 0.65. At this layer distance the particles in the two layers conspire to realize a structure similar to the one which would be obtained if they were in a common plane.

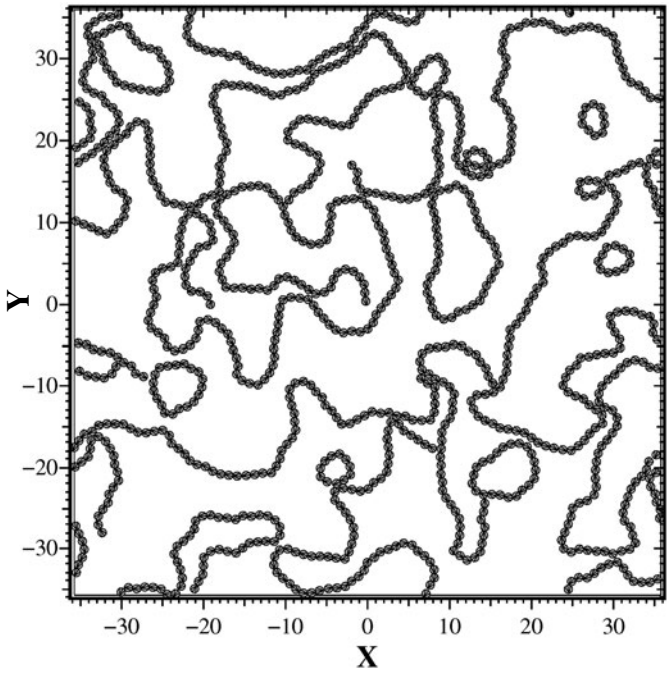

Figure 3. Snapshot of a configuration of 1024 Q2D dipolar hard spheres at density $\rho^* = 0.20$ and dipole moment $\mu^* = 2.75$. The box lengths are in units of σ.

For layer distances $h > 2\sigma$ the structures in both layers are largely uncorrelated. A detailed account of bilayer structure will appear in [124].

If the dipolar spheres move in monolayers or bilayers separating regions of different dielectric constants (e.g., phospholipid monolayers at an air–water interface) polarization charges on the interface need to be taken into account (e.g. through image charges). According to [125], presenting simulations of a monolayer of dipolar hard spheres at the interface of two media of different dielectric constants, even a small ratio $\Delta \sim 5$ of the two dielectric constants seems sufficient to destroy chaining present at $\Delta = 1$. Moreover, for $\Delta \sim 40$ (typical of a water–heptane interface), the dipole moments are found to orient perpendicular to the interface rather than parallel when $\Delta = 1$.

4. Dipolar systems in an external field

The possibility of direct visualization, e.g. through video microscopy, makes Q2D microsized colloidal suspensions particularly suited for studying experimentally formation of ordered structures or melting mechanisms in 2D systems. If a layer of dipoles is subject to an external field, depending on whether the external field is perpendicular or parallel to the layer, the dipoles will repel or attract each other giving rise to completely different structures.

In a sufficiently strong external electric or magnetic field, perpendicular to the layer, the colloidal particles interact, to a good approximation, through a repulsive long-range $1/r^3$ potential and self-assemble, when confined by walls or magnetic fields, into different planar lattice structures. Triangular (hexagonal) [87–89, 126–128] but also rectangular, square or oblique lattices (some of which are metastable) have been observed [89].

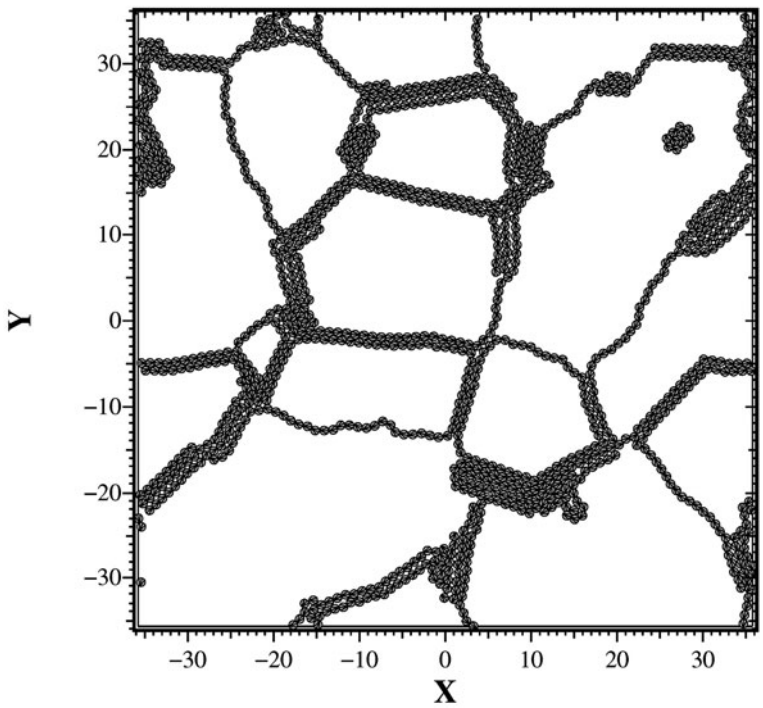

Figure 4. Snapshot of a configuration of 1024 Q2D dipolar hard spheres with attractive Yukawa potential $-\epsilon\frac{e^{-z(r-\sigma)}}{r/\sigma}$ at density $\rho^* = 0.20$ and dipole moment $\mu^* = 2.75$. The strength of the Yukawa potential is $\epsilon/kT = 3.78$ and $z\sigma = 2$. The simulation was started from an equilibrated configuration at $\epsilon = 0$. It should be noted, however, that once the particles have assembled in the structure shown, the acceptance rate of single-particle MC trial moves gets very low and the system remains pinned down in that peculiar configuration. The box lengths are in units of σ.

Melting of the crystal structures has been observed in micrometre-sized colloids confined between glass plates [90] or confined by gravity to a water/air interface [91] and shown to consist of two successive transitions, with an intermediate hexatic phase, as predicted by the KTHNY theory [129–131]. Evidence for hexatic-to-liquid melting has also been given in 2D magnet bubble lattices in magnetic garnet films [17]. These experimental observations are in disagreement with numerical simulations of systems with $1/r^3$ potentials which report first-order melting [132, 133].

Melting of 2D clusters of up to 80 dipoles, interacting with a $1/r^3$ potential, confined by a quadratic potential has been investigated by means of MC simulations by Belousov and Lozovik [134]. Melting of the smaller clusters (size $N < 37$) differs from that of the larger ones through an additional stage characterized by orientational intershell disordering of different pairs of shells.

Orientational fluctuations of the dipole moments in the direction perpendicular to the layer have been investigated in MC simulations by Lomba *et al* [135] as a function of density and strength of the perpendicular magnetic field. They show, in particular, that an inhomogeneous Ornstein–Zernike equation [136], coupling pair correlation functions to the one-particle orientational distribution function $f(\cos\theta)$, where θ is the angle the dipole moment makes with the layer normal, provides an accurate description of the spatial and orientational structure of a monolayer of paramagnetic spherical particles in an external field.

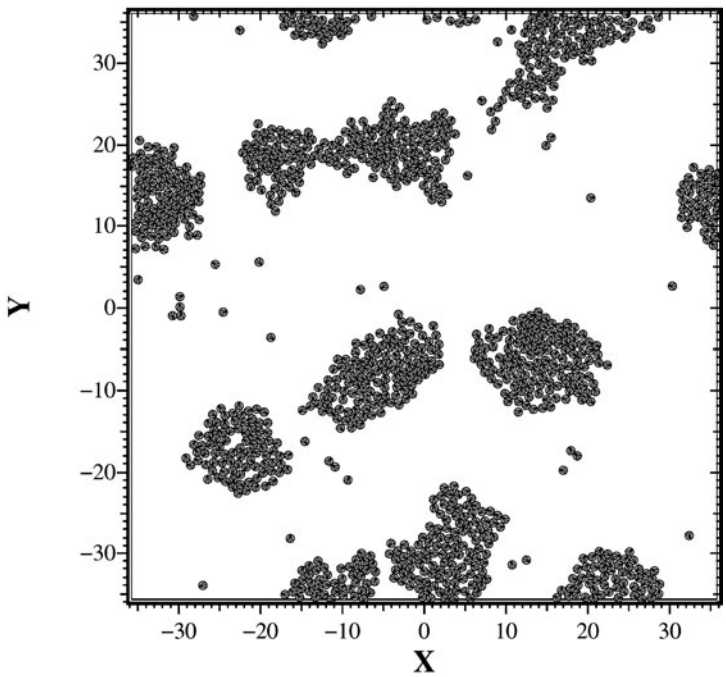

Figure 5. Snapshot of a configuration of 1024 Q2D dipolar hard spheres with attractive Yukawa potential at density $\rho^* = 0.20$ and dipole moment $\mu^* = 1.5$. The strength of the Yukawa potential is $\epsilon/kT = 3.78$ and $z\sigma = 2$. The box lengths are in units of σ.

Dynamical aspects of Q2D suspensions of spherical colloids and asymmetric colloid mixtures with long-range repulsive forces have been investigated by Brownian dynamics simulations [137–139]. These works emphasize dynamic scaling and the importance of hydrodynamic interactions on self- and tracer diffusion.

If, instead, a field is applied parallel to the layer, the energetically most favourable arrangement of Q2D dipolar spheres is association into chainlike structures parallel to the direction of the field [102, 140, 141]. MC simulations of Q2D ferromagnetic colloidal dispersions modelled as dipolar hard spheres of equal size and dipole strength, in a magnetic field H, were performed by Satoh *et al* [78] to investigate the influence of the dipole moment and field strength on the formation of chainlike aggregates. Additional MC simulation results for a system of 1872 dipolar spheres in a field of strength $h = \frac{\mu H}{kT} = 10$ are shown in figures 9–13. Above a certain value of the dipole moment the dipolar spheres aggregate into chains which align in the direction of the field. At low density, $\rho^* = 0.05$, (figure 9) the chains are isolated and of various lengths. At higher densities ($\rho^* = 0.2$) the chains span the simulation cell and coalesce to form thicker, more or less regularly spaced clusters (columns) involving two or three chains at $\rho^* = 0.2$ and four to six chains at $\rho^* = 0.4$. At dipole moment $\mu^* = 2.5$ (figures 10 and 11) the columns are rather sluggish with defects and branching. From figure 11 it is apparent that chains can tilt away from the field and be attracted to another column (zippering [142]). By increasing the dipole moment the columns get more rigid but still contain defects (figures 12 and 13). Neighbouring chains in a column are seen (figure 13) to be displaced by one hard-sphere radius giving an attraction between the chains [143, 144] (see below).

A richer variety of structures occurs in the physically more relevant 2D + h systems as realized experimentally, e.g., in suspensions of dielectric particles in a nonconducting (or

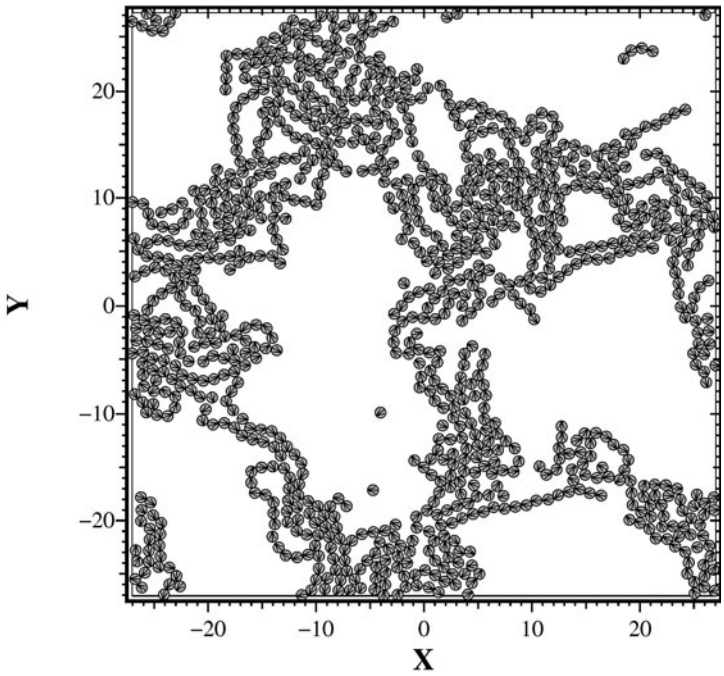

Figure 6. Snapshot of a configuration of 1024 Q2D dipolar hard spheres with attractive Yukawa potential for $\rho^* = 0.35$, $\mu^* = 2.24$, $\epsilon/kT = 2.25$ and $z\sigma = 2$. The box lengths are in units of σ.

weakly conducting) solvent (ER fluids) or magnetizable particles in a nonmagnetic liquid (MR fluids). If the permittivity or permeability mismatch between the particles and the suspending medium is sufficiently large the electric or magnetic field will induce a dipole moment within the particles proportional to the local field they experience. Recent experiments on ER fluids by Dassanayaka *et al* [145] reveal that, depending on volume fraction, electrode gap, strength and ramping rate of the applied field as well as starting conditions (particles sedimented under gravitation or dispersed through the surrounding medium), the system can form chains, (metastable) sheets of hexagonally ordered 2D structures aligned with the external field, forming an interconnected labyrinthine arrangement, columns or domains of body-centred tetragonal (bct) crystals. Quite remarkably, similar structures, including the sheet arrangement, have also been observed in simulation studies [142, 146].

If a slowly increasing *magnetic* field is applied to a ferrofluid emulsion it changes through a sequence of structures which have been described as follows [147, 148]: at low field the particles are randomly distributed (gas). When the dipole moment exceeds the thermal energy short chains of variable lengths form in coexistence with single particles. At a characteristic value of the field long chains spanning the sample start to absorb the neighbouring short chains thereby forming columns. With increasing field these loosely bound columns transform to nearly equally sized and spaced densely packed solid-like columns [147].

At high rates of application of the magnetic field additional nonequilibrium states form which have been characterized as bent-wall-like and labyrinthine structures [149]. These are metastable states in which the structures are locked in one of the local minima of the energy landscape.

A theoretical understanding of the structures detailed above largely rests on the knowledge of the lateral interactions between dipolar chains as they govern the coalescence of the chains

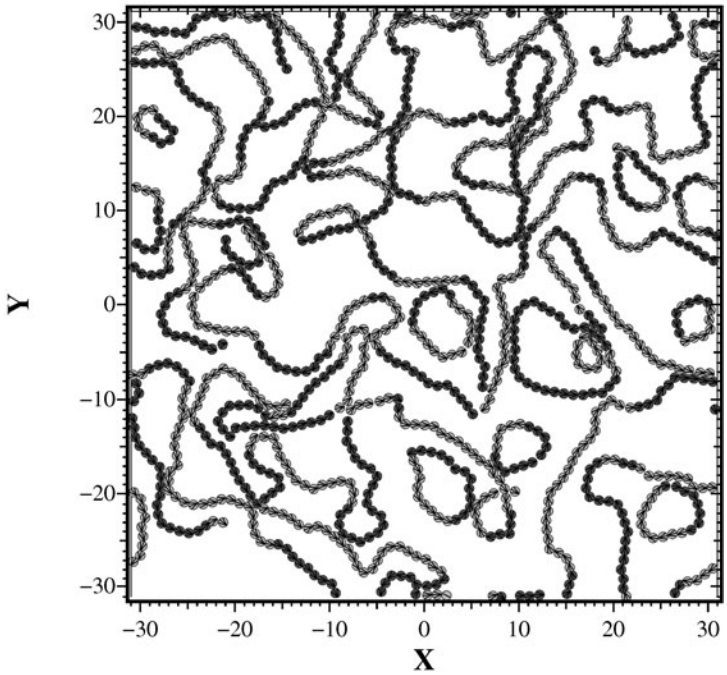

Figure 7. Snapshot of a configuration (projected on the xy-plane) of a bilayer of Q2D dipolar hard spheres obtained with the EW2D + h method. The layer separation is $h = 0.5\sigma$. Each layer contains 576 particles at density $\rho^* = 0.15$ and dipole moment $\mu^* = 2.75$. Dark and light colours refer to particles in the two different layers, respectively. Arrows represent the projections of the dipole moments on the xy-plane. Dimensions along the x- and y-axes are in units of σ.

into more compact structures. A distinction has to be made between ER and MR fluids, due to the different boundaries, in the experimental setups, at the confining surface perpendicular to the applied field. In ER fluids the system is confined between parallel conducting electrodes at fixed potential. The electric field created by a chain spanning the electrodes is therefore that of an effectively infinite chain resulting from combining the particles with their infinite series of images in order to guarantee vanishing of the tangential component of the electric field at the surface [143, 150]. For a perfectly ordered monodisperse chain this field decays exponentially with lateral distance so that chains separated by a distance much larger than their interparticle spacing do not interact strongly. Chains in register will repel one another whereas chains displaced with respect to another in the direction of the field can experience an attractive interaction. However, in view of their short-range nature these attractive interactions are not expected to be the only ones to drive formation of columns and coarsening. Thermal fluctuations of the chains [151–153] and chain defects [142, 154] creating a local variation in the dipole moment density along a chain are processes which induce interactions that drive lateral coalescence. A good summary of the dominant mechanisms of lateral interaction as a function of dipole strength and volume fraction is given in [155].

In MR fluids, where particles are confined by cell walls of low permeability (e.g. glass), demagnetization field effects are important [147, 148, 156], in contrast to the ER case. Chains have finite length and therefore interactions can have a longer range than for the perfect infinite chain case [157]. Effective magnetic charges (monopoles) arising from the demagnetization effect on the ends of the chains and columns cause a repulsion which is believed to be

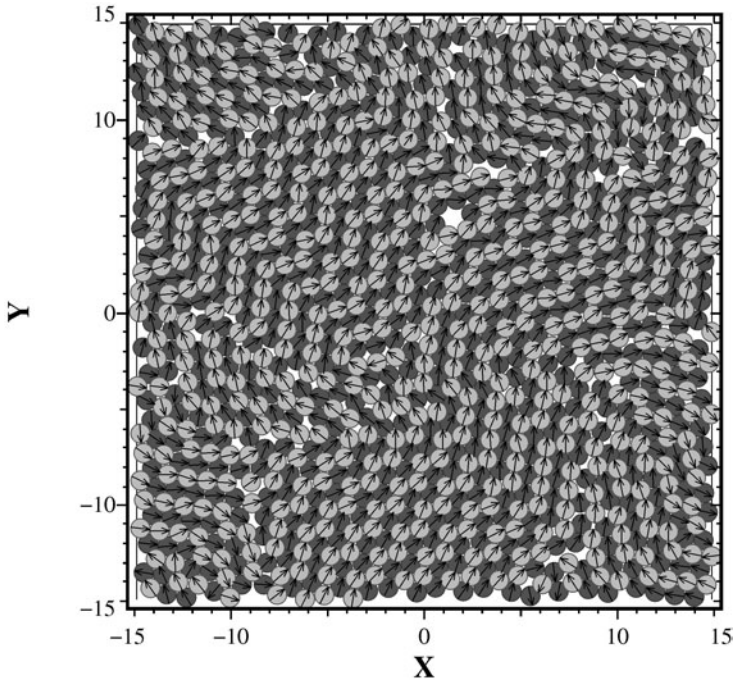

Figure 8. The same as figure 7 but for $\rho^* = 0.65$.

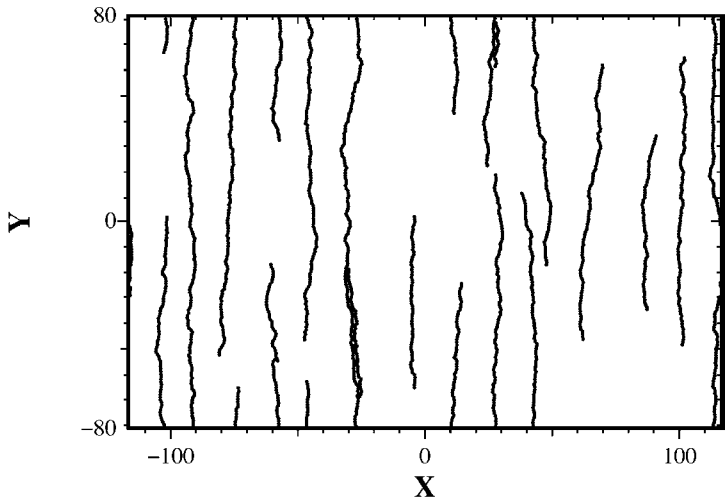

Figure 9. Snapshot of a configuration of 1872 Q2D dipolar hard spheres in an external field of strength $h = \mu H/kT = 10$ parallel to the y-axis. The density is $\rho^* = 0.05$ and the dipole moment $\mu^* = 2.5$. The box lengths are in units of σ.

responsible for the local ordering of the colums as well as the tapered or split ends of the columns [147]. Calculations and experiments show that the ground state consists of spheroidal (ellipsoidal) clusters inside which the particles are arranged in a bct structure [156], in contrast to ER where a bct crystal minimizes the energy [158–162].

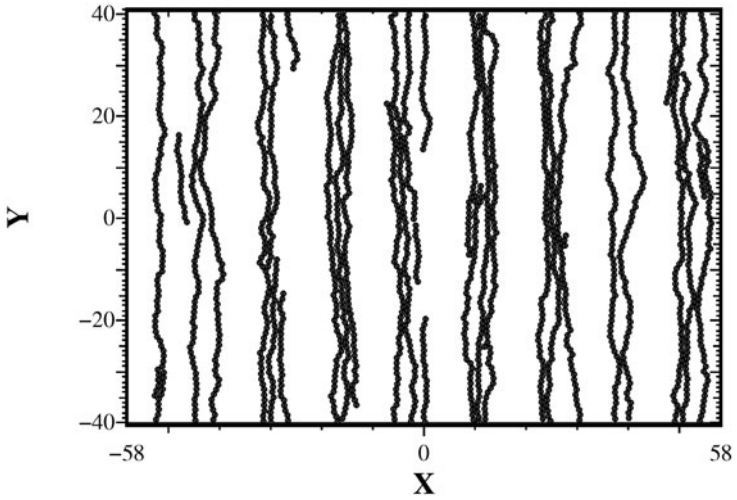

Figure 10. The same as figure 9 but for density $\rho^* = 0.2$ and dipole moment $\mu^* = 2.5$. The box lengths are in units of σ.

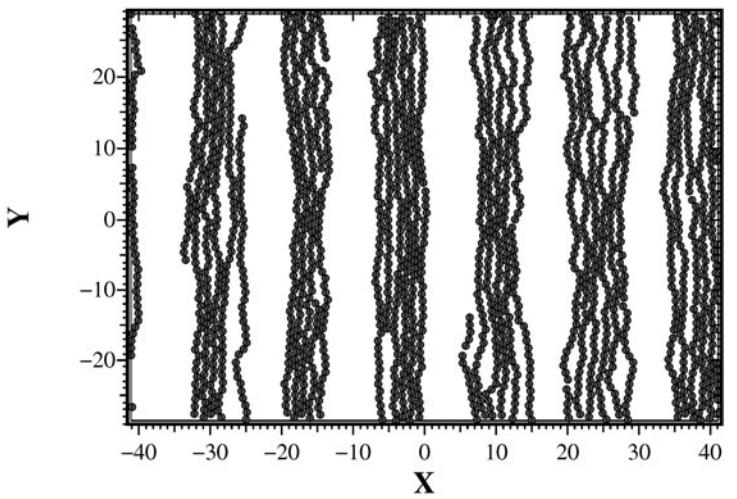

Figure 11. The same as figure 9 but for density $\rho^* = 0.4$ and dipole moment $\mu^* = 2.5$. The box lengths are in units of σ.

5. Thin magnetic films

Thin magnetic films, for instance thin metal films grown on metal substrates (Fe on Cu(100) or Co on Au(111)), exhibit a variety of orientationally ordered phases depending on temperature and thickness. In systems a few monolayers thick, the magnetization generally occurs preferentially perpendicular to the film plane at low temperature [10, 12]. As the temperature is increased, domains form with reverse, mainly perpendicular, orientations of the spins to give an essentially zero net magnetization. As the temperature is further increased the spins orient parallel to the film and at still higher temperatures the system is paramagnetic. In most systems, increasing the film thickness at fixed temperature has a similar effect to raising the

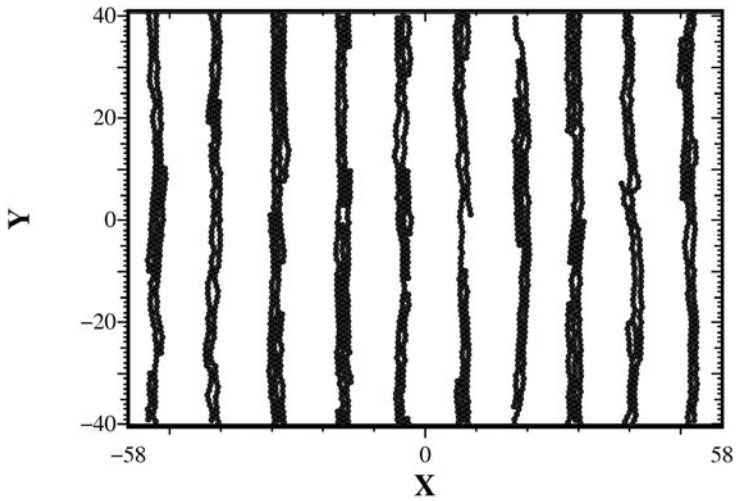

Figure 12. The same as figure 9 but for density $\rho^* = 0.2$ and dipole moment $\mu^* = 3$. The box lengths are in units of σ.

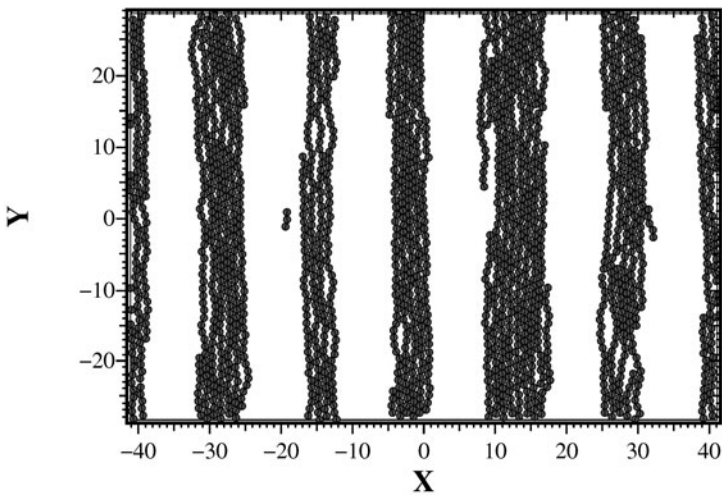

Figure 13. The same as figure 9 but for density $\rho^* = 0.4$ and dipole moment $\mu^* = 2.75$. The box lengths are in units of σ.

temperature [14, 15] (an exception is Ni on Cu(001) [163]). In Co films, for instance, for films thicker than about seven monolayers, the surface anisotropy is no longer sufficient to overcome the dipole–dipole interaction and the magnetization switches from perpendicular to parallel to the film. Interestingly, in the range of 10–50 nm thickness, the magnetization orients again perpendicular to the film and above 50 nm formation of domains, bubbles and stripes, is observed [15, 164].

The model (1) involving exchange, dipolar and single-site effective anisotropy interactions has been widely used to study reorientation and formation of stripe phases in continuous or granular uniaxial thin magnetic films [12]. As already pointed out in section 3 the sole dipolar interaction causes the spins to lie preferentially parallel to the film layer at low temperature.

The effect of the anisotropy term in (1) is to orient them out of plane. If K is large compared to the dipole coupling g, the spins will be nearly perpendicular to the film plane in which case the dipole interaction will be dominated by the isotropic contribution, $\frac{g}{r_{ij}^3}\boldsymbol{s}_i \cdot \boldsymbol{s}_j$, favouring antiferromagnetic ordering of the spins. In this event, the interplay of the long-range dipolar interaction and the short-range exchange interaction, when g is comparable to J, is at the origin of formation of stripe domains. Depending on the relative strengths of the various coupling constants a large variety of phases is therefore expected [12, 16].

The ground state configurations associated with model (1), obtained for a square lattice by a simulated annealing procedure in a wide range of the parameters J/g and K/g [165], already reproduce qualitatively most of the different magnetic patterns observed in experiment. The finite-temperature phase diagrams have been characterized most comprehensively by MC simulations of spins on a 40×40 square lattice by MacIsaac and collaborators [12]. Depending on whether the exchange coupling is smaller than, comparable to or larger than the dipole interaction, different phase behaviour is observed in the (temperature, K/g)-plane. If the exchange interaction is small ($J \ll g$), a first-order reorientation transition from an antiferromagnetically ordered in-plane to an antiferromagnetically ordered out-of-plane phase occurs with increasing values of the anisotropy K/g at low temperature [166]. When exchange and dipolar interactions compete ($J \sim g$), in accord with the qualitative reasoning given above, stripe domains are observed above some value of K/g depending on temperature. The reorientation transition from the in-plane ferromagnetic phase at low K to the out-of-plane stripe phase is again first order [167]. The width of the stripes increases with J, in accord with ground state calculations [167, 168]. For large values of K and low temperature the stripes are highly ordered and aligned along one of the axes of the square lattice [167, 169]. As the temperature increases, due to fluctuations of the domain walls, the system breaks up into extended domains of irregular shape in which the spins are nevertheless highly ordered, spins in adjacent domains pointing in opposite directions perpendicular to the film plane (tetragonal phase) [167]. Such domains have also been found in off-lattice MC simulations [29]. Only at still higher temperatures does the system disorient. It should be remarked, however, that the phase behaviour can depend on the underlying lattice structure. Lattice simulations of a disc-shaped sample of 10 200 spins on a triangular lattice with free boundary conditions [170] give evidence, at very low temperature, of a complex domain pattern characterized by a twisted spin structure (the magnetization rotates in a helicoidal way along the three principal axes). This structure occurs when the anisotropy energy equals the dipolar energy and separates the out-of-plane domain phase at high K/g from the in-plane vortex phase [98] at low K/g.

For $J \gg g$, the width of the stripe domains may be larger than the system size of the simulations and a single ferromagnetic domain is observed. It should be noted, however, that the dipolar interaction always destabilizes the ferromagnetic state against formation of an antiferromagnetic stripe phase, regardless of the strength of the exchange interaction [171].

The order of the reorientation transition depends sensitively on the precise form of the anisotropy energy and therefore film thickness [172]. For (uniaxial) monolayers for which an anisotropy of the form shown in equation (1) seems most appropriate the transition is first order. In few-layer systems the anisotropy 'constant' K is likely to be layer dependent. Lattice MC simulations for a square two-layer system, with different values of K in the two layers, show that in this case the reorientation transition is second order [122].

Stripe melting has been studied most thoroughly by Stoycheva and Singer [74] on a hexagonal lattice for an Ising spin type model (limit $K \to \infty$ of equation (1))

$$H = -J \sum_{\langle i,j \rangle} s_i s_j + \frac{1}{2} g \sum_{i \neq j} \frac{s_i s_j}{r_{ij}^3} \tag{26}$$

where $s_i \pm 1$ are Ising spin variables and J, $g > 0$. The sum over spins in the first term of the rhs of (26) is over nearest neighbours while that in the second term extends over all spins in the system. A hexagonal lattice has been chosen in preference to a square one to reduce the effect of symmetry breaking caused by the underlying lattice structure.

The stripe width is essentially governed by the ratio J/g scaling as $\sim e^{J/g}$ [74, 171] and the melting temperature moves up with increasing values of J/g (decrease of the repulsion). For large values of J/g large simulation systems are thus required to accommodate long-wave-modulated phases. Stoycheva and Singer [74] use more than a hundred thousand spins allowing them to cover the range $0.27 < g/J < 0.43$. For such a large number of spins, conventional Ewald sums would be prohibitively costly and, as mentioned in section 2, only FMM or PME type methods can cope with such large systems. Stoycheva and Singer [74] adapted the FMM originally proposed by Greengard and Rokhlin [70] to the triangular lattice case. A second difficulty encountered in these simulations is the extremely slow equilibration of the domain boundaries at the low temperatures where the stripe phase exists. For the short-range Ising model, where a similar problem arises near the ferromagnetic transition, the difficulty can be alleviated by using cluster algorithms, most efficiently the Wolff algorithm [173]. Unfortunately it is not applicable to the *long-range* Ising model. Stoycheva and Singer circumvent the problem by implementing a variant of a cluster update algorithm proposed by Creutz [174] and sampling spins preferentially in the region of domain walls. A major conclusion of their simulation work is that in the range of g/J values where reliable results could be obtained the melting is mediated by topological defect unbinding [129]. They point out, however, that at lower values of g/J where the melting temperature approaches that of the bare Ising model critical temperature, it cannot be excluded that melting occurs by disordering of the spins within the domains as predicted by an analytic theory [175].

Recently the phase behaviour of Q2D lattice systems with antiferromagnetic exchange coupling ($J < 0$) has been investigated as well. In the absence of anisotropy ($K = 0$) the competition between the antiferromagnetic exchange and the dipolar interaction induces a reorientation transition from an in-plane antiferromagnetic to an out-of-plane antiferromagnetically ordered phase [176]. On the other hand MC simulations for $K < 0$ (easy axis parallel to the plane) give evidence for two types of antiferromagnetic domain, Bloch and Néel domains [177].

As a last example we shall mention a simulation study [178] of the ground state magnetic properties of nanoparticles (nanometre-sized single-domain ferromagnetic (e.g. Co) particles [22, 25]). When well coated and deposited on a substrate, nanoparticles spontaneously self-assemble in 2D hexagonal networks [22, 23]. As in these systems exchange can be neglected, the orientational structure results from competition between the dipolar interaction and the anisotropy which favours a disordered state when the easy axes are distributed randomly. Upon increase of the dipolar interaction the orientational structure is shown to vary from a disordered (out-of-plane) state to an in-plane ordered state. Although the ordered state depends on the lattice structure (ferromagnetic for a hexagonal lattice, antiferromagnetic for a square lattice) the magnetic properties are shown not to do so.

6. Conclusion

From this brief review, primarily centred on MC simulations, it is readily apparent that Q2D dipolar systems, alone or in combination with other interactions, present a rich variety of structures, phases and phase transitions. Simulations on a microscopic scale, continuum and lattice, essentially based on a Hamiltonian given by equation (1), have certainly contributed to our theoretical understanding of these phases, if only through the possibility of allowing an

easier control than in experiment of the different couplings that can conspire in phase formation. Equation (1) may nevertheless be too crude for quantitative predictions (the anisotropy term is very approximate [172], the point dipole approximation is insufficient to accurately predict the properties of ER fluids [179], polydispersity is neglected etc).

Simulations of strongly interacting dipolar systems are, however, not without difficulty. Due to the strong association of the particles at low temperature, single MC trial moves will have low acceptance rates and the system can easily be trapped for long times in local energy minima. In low-density systems, where aggregates are well separated, cluster moves can alleviate this difficulty, while in more dense systems hyperparallel tempering [180] may be helpful to avoid the system getting pinned down in a peculiar configuration.

As we have seen in the context of thin magnetic films, pattern formation can occur on a length scale approaching or exceeding system sizes for which energies can be evaluated by the usual Ewald method without running into prohibitively large computing times. Large system sizes are also required for a precise location, through a finite-size scaling analysis [181], of reorientation transitions. In these circumstances, FMM and PME approaches are alternatives to the usual Ewald method but are less straightforward to implement.

Another difficulty manifests in phase transitions associated with domain morphologies [74]. Efficient sampling of the domains would require a cluster update algorithm similar to the Wolff algorithm which allows us to overcome critical slowing down in the short-range Ising model. Unfortunately, an algorithm comparable in efficiency to the Wolff procedure is not yet available for long-range potentials.

We have shown that energy and pair correlation functions of a bilayer of dipolar hard spheres can be accurately evaluated using the usual EW3D method. This may stimulate further simulation studies of the role of electrostatic interactions between planar dipolar surfaces across dielectric media [182, 183] (lamellae of surfactants, clay platelets, . . .) or magnetization properties of few-layer thin magnetic films [184, 185]. Work in this direction is in progress.

References

[1] Maleev S V 1966 *Sov. Phys.–JETP* **43** 1240
[2] Beier T, Jahrreis H, Pescia D, Woike Th and Gudat W 1988 *Phys. Rev. Lett.* **61** 1875
[3] Malozovsky Yu M and Rozenbaum V M 1991 *Physica* A **175** 127
[4] Bedanov V M 1992 *J. Phys.: Condens. Matter* **4** 75
[5] De'Bell K, MacIsaac A B, Booth I N and Whitehead J P 1997 *Phys. Rev.* B **55** 15108
[6] Rastelli E, Carbognani A, Regina S and Tassi A 1999 *J. Appl. Phys.* **85** 6082
[7] Carbognani A, Rastelli E, Regina S and Tassi A 2000 *Phys. Rev.* B **62** 1015
[8] Rastelli E, Regina S, Tassi A and Carbognani A 2002 *Phys. Rev.* B **65** 094412
[9] Pappas D P, Kämper K P and Hopster H 1990 *Phys. Rev. Lett.* **64** 3179
[10] Allenspach R and Bischof A 1992 *Phys. Rev. Lett.* **69** 3385
[11] Allenspach R 1994 *J. Magn. Magn. Mater.* **129** 160 and references therein
[12] De'Bell K, MacIsaac A B and Whitehead J P 2000 *Rev. Mod. Phys.* **72** 225
[13] Seul M and Andelman D 1995 *Science* **267** 476
[14] Allenspach R, Stampanoni M and Bischof A 1990 *Phys. Rev. Lett.* **65** 3344
[15] Hehn M, Padovani S, Ounadjela K and Bucher J P 1996 *Phys. Rev.* B **54** 3428
[16] Politi P 1998 *Comments Condens. Matter Phys.* **18** 191
[17] Seshadri R and Westervelt R M 1992 *Phys. Rev.* B **46** 5142
[18] Seul M and Wolfe R 1992 *Phys. Rev.* A **46** 7519
[19] McConnell H M, Tamm L K and Weis R M 1984 *Proc. Natl Acad. Sci. USA* **81** 3249
[20] Seul M and Sammon M J 1990 *Phys. Rev. Lett.* **64** 1903
[21] Seul M 1990 *Physica* A **168** 198
[22] Petit C, Taleb A and Pileni M P 1999 *J. Phys. Chem.* B **103** 1805
[23] Sun S and Murray C B 1999 *J. Appl. Phys.* **85** 4325
[24] Puntes V F, Krishnan K M and Alivisatos A P 2001 *Appl. Phys. Lett.* **78** 2187

[25] Puntes V F, Krishnan K M and Alivisatos A P 2001 *Science* **291** 2115
[26] Rosensweig R E 1985 *Ferrohydrodynamics* (New York: Cambridge University Press)
[27] Tojima A, Manaka T and Iwamoto M 2001 *J. Chem. Phys.* **115** 9010
[28] Allen M P and Tildesley D J 1989 *Computer Simulation of Liquids* (Oxford: Clarendon)
[29] Weis J J 2002 *Mol. Phys.* **100** 579
[30] Aharoni A 1996 *Introduction to the Theory of Ferromagnetism* (Oxford: Clarendon)
[31] Shelley J C and Patey G N 1996 *Mol. Phys.* **88** 385
[32] Gao G T, Zeng X C and Wang W 1997 *J. Chem. Phys.* **106** 3311
[33] Perram J W and de Leeuw S W 1981 *Physica* A **109** 237
[34] Wei D and Patey G N 1992 *Phys. Rev.* A **46** 7783
[35] Weis J J and Levesque D 1993 *Phys. Rev.* E **48** 3728
[36] Smith E R 1982 *Mol. Phys.* **45** 915
[37] Caillol J M 1992 *J. Chem. Phys.* **96** 1455
[38] Caillol J M, Levesque D and Weis J J 1981 *Mol. Phys.* **44** 733
[39] Parry D E 1975 *Surf. Sci.* **49** 433
[40] Parry D E 1975 *Surf. Sci.* **64** 195
[41] Heyes D M 1994 *Phys. Rev.* B **49** 755
[42] Grzybowsi A, Gwóźdź E and Bródka A 2000 *Phys. Rev.* B **61** 6706
[43] Mecke M, Fischer J and Winkelmann J 2000 *J. Chem. Phys.* **114** 5842
[44] Spohr 1997 *J. Chem. Phys.* **107** 6342
[45] Yeh I C and Berkowitz M L 1999 *J. Chem. Phys.* **111** 3155
[46] Frenkel D and Smit B 1996 *Understanding Molecular Simulation* (San Diego, CA: Academic)
[47] Arnold A, de Joannis J and Holm C 2002 *J. Chem. Phys.* **117** 2496
[48] de Joannis J, Arnold A and Holm C 2002 *J. Chem. Phys.* **117** 2503
[49] Bródka A and Grzybowski A 2002 *J. Chem. Phys.* **117** 8208
[50] Hautman J and Klein M L 1992 *Mol. Phys.* **75** 379
[51] Pellenq R J M, Caillol J M and Delville A 1997 *J. Phys. Chem.* B **101** 8584
[52] Allahyarov E, D'Amico I and Löwen H 1999 *Phys. Rev.* E **60** 3199
[53] Mazars M, Caillol J M, Weis J J and Levesque D 2001 *Condens. Matter. Phys.* **4** 697
[54] Lekner J and Castle P J 1980 *Physica* A **101** 89
[55] Lekner J 1989 *Physica* A **157** 826
[56] Arnold A and Holm C 2002 *Chem. Phys. Lett.* **354** 324
[57] De Leeuw S W and Perram J W 1979 *Mol. Phys.* **37** 1313
[58] Smith E R 1988 *Mol. Phys.* **65** 1089
[59] Kjellander R 1984 *J. Chem. Soc. Faraday Trans.* II **80** 1323
[60] Warner M and Hornreich 1985 *J. Phys. A: Math. Gen.* **18** 2325
[61] Gulley G L and Tao R 1997 *Phys. Rev.* E **56** 4328
[62] Yu K W and Wan J T K 2000 *Comput. Phys. Commun.* **129** 177
[63] Hautman J, Halley J W and Rhee Y J 1989 *J. Chem. Phys.* **91** 467
[64] Perram J W and Ratner M A 1996 *J. Chem. Phys.* **104** 5174
[65] Perram J W, Petersen H G and de Leeuw S W 1988 *Mol. Phys.* **65** 875
[66] Toukmaji A Y and Board J A 1996 *Comput. Phys. Commun.* **95** 73
[67] Hockney R W and Eastwood J W 1988 *Computer Simulations Using Particles* (Bristol: Institute of Physics Publishing)
[68] Essmann U, Perera L, Berkowitz M L, Darden T, Lee H and Pedersen L G 1995 *J. Chem. Phys.* **103** 8577
[69] Deserno M and Holm C 1998 *J. Chem. Phys.* **109** 7678
[70] Greengard L and Rokhlin V 1987 *J. Comput. Phys.* **73** 325
[71] Ding H Q, Karasawa N and Goddard W A III 1992 *J. Chem. Phys.* **97** 4309
[72] Kutteh R and Nicholas J B 1995 *Comput. Phys. Commun.* **86** 236
[73] Toukmaji A Y, Sagui C, Board J A and Darden T 2000 *J. Chem. Phys.* **113** 10913
[74] Stoycheva A D and Singer S J 2002 *Phys. Rev.* E **63** 036706
[75] Kawata M and Nagashima U 2002 *Chem. Phys. Lett.* **340** 165
[76] Wu D, Chandler D and Smit B 1992 *J. Phys. Chem.* **96** 4077
[77] Tavares J M, Weis J J and Telo da Gama M M 1999 *Phys. Rev.* E **59** 4388
[78] Satoh A, Chantrell R W, Kamiyama S-I and Coverdale G N 1996 *J. Colloid Interface Sci.* **178** 620
[79] Coverdale G N, Chantrell R W, Martin G A R, Bradbury A, Hart A and Parker D A 1998 *J. Magn. Magn. Mater.* **188** 41
[80] Davis S W, McCausland W, McGahagan H C, Tanaka C T and Widom M 1999 *Phys. Rev.* E **59** 2424

[81] Tavares J M, Weis J J and Telo da Gama M M 2002 *Phys. Rev.* E **65** 061201
[82] Kaganar V M, Möwald H and Dutta P 1999 *Rev. Mod. Phys.* **71** 779
[83] Andelman D, Brochard F, Knobler C and Rondelez F 1994 *Micelles, Membranes, Microemulsions and Monolayers* ed W M Gelbart, A Ben-shaul and D Roux (New York: Springer)
[84] Andelman D, Brochard F and Joanny J-F 1987 *J. Chem. Phys.* **86** 3673
[85] Keller D J, McConnell H M and Moy V T 1986 *J. Phys. Chem.* **90** 2311
[86] Schneider K P and Keller J 1997 *Chem. Phys. Lett.* **275** 63
[87] Skjeltorp A T 1983 *Phys. Rev. Lett.* **51** 2306
[88] Golosovsky M, Saado Y and Davidov D 1999 *Appl. Phys. Lett.* **75** 4168
[89] Wen W, Zhang L and Sheng P 2000 *Phys. Rev. Lett.* **85** 5464
[90] Kusner R E, Mann J A and Dahm A J 1995 *Phys. Rev.* B **51** 5746
[91] Zahn K, Lenke R and Maret G 1999 *Phys. Rev. Lett.* **82** 2721
[92] Gil-Villegas A, McGrother S C and Jackson G 1997 *Chem. Phys. Lett.* **269** 441
[93] Brankov J G and Danchev D M 1987 *Physica* A **144** 128
[94] Belobrov P I, Gekht R S and Ignatchenko V A 1983 *Sov. Phys.–JETP* **57** 636
[95] Henley C L 1989 *Phys. Rev. Lett.* **62** 2056
[96] Prakash S and Henley C L 1990 *Phys. Rev.* B **42** 6574
[97] Olive E and Molho P 1998 *Phys. Rev.* B **58** 9238
[98] Vedmedenko E Y, Ghazali A and Lévy J-C S 1999 *Phys. Rev.* B **59** 3329
[99] Weis J J, Tavares J M and Telo da Gama M M 2002 *J. Phys.: Condens. Matter* **14** 9171
[100] Weis J J 1998 *Mol. Phys.* **93** 361
[101] Wen W, Pál K F, Zheng D W and Tu K N 1999 *Phys. Rev.* E **59** R4758
[102] Butter K, Vroege G J, Philipse A P, Bomans P H and Frederik P M 2003 *J. Phys.: Condens. Matter* **14**
[103] de Gennes P G 1979 *Scaling Concepts in Polymer Physics* (Ithaca, NY: Cornell University Press)
[104] Wittmer J P, Milchev A and Cates M E 1998 *J. Chem. Phys.* **109** 834
[105] Wittmer J P, van der Schoot P, Milchev A and Barrat J L 2000 *J. Chem. Phys.* **113** 6992
[106] Helgesen G, Skjeltorp A T, Mors P M, Botet R and Jullien R 1988 *Phys. Rev. Lett.* **61** 1736
[107] Liu B X and Ding J R *Phys. Rev.* B **40** 7432
[108] Yang F and Pan F 2001 *Phys. Rev.* E **64** 051402
[109] Trohidou K N and Blackman J A 1995 *Phys. Rev.* B **51** 11521
[110] Pastor-Satorras R and Rubi J M 1995 *Phys. Rev.* E **51** 5994
[111] Morimoto H and Maekawa T 2000 *J. Phys. A: Math. Gen.* **33** 247
[112] Teixeira P I C, Tavares J M and Telo da Gama M M 2000 *J. Phys.: Condens. Matter* **12** R411
[113] Camp P J and Patey G N 2000 *Phys. Rev.* E **62** 5403
[114] Tlusty T and Safran S A 2000 *Science* **290** 1328
[115] Zilman A G and Safran S A 2002 *Preprint* cond-mat/0205488
[116] Sear R P and Cuesta J 2001 *Europhys. Lett.* **55** 451
[117] Cuesta J A and Sear R P 2002 *Phys. Rev.* E **65** 031406
[118] van Leeuwen M E and Smit B 1993 *Phys. Rev. Lett.* **71** 3991
[119] Rein ten Wolde, Oxtoby D W and Frenkel D 1999 *J. Chem. Phys.* **111** 4762
[120] Lefebure S, Ménager C, Cabuil V, Assenheimer M, Gallet F and Flament G 1998 *J. Phys. Chem.* B **102** 2733
[121] Klapp S H L and Schoen M 2002 *J. Chem. Phys.* **117** 8050
[122] Hucht A and Usadel K D 1996 *J. Magn. Magn. Mater.* **156** 423
[123] Saiz L and Klein M L 2002 *J. Chem. Phys.* **116** 3052
[124] Weis J J unpublished
[125] Zarragoicoechea G J 1999 *Mol. Phys.* **96** 1109
[126] Pieranski P 1980 *Phys. Rev. Lett.* **45** 569
[127] Skjeltorp A T and Helgesen G 1991 *Physica* A **176** 37
[128] Helgesen G and Skjeltorp A T 1991 *Physica* A **180** 488
[129] Kosterlitz J M and Thouless D J 1973 *J. Phys. C: Solid State Phys.* **6** 1181
[130] Nelson D R and Halperin B I 1979 *Phys. Rev.* B **19** 2457
[131] Young A P 1979 *Phys. Rev.* B **19** 1855
[132] Kalia R K and Vashishta P 1981 *J. Phys. C: Solid State Phys.* **14** L643
[133] Bedanov V M, Gadiyak G V and Lozovik Yu E 1982 *Phys. Lett.* A **92** 400
[134] Belousov A I and Lozovik Yu E 2000 *Eur. Phys. J.* D **8** 251
[135] Lomba E, Lado F and Weis J J 2000 *Phys. Rev.* E **61** 3838
[136] Evans R 1992 *Fundamentals of Inhomogeneous Fluids* ed D Henderson (New York: Dekker)
[137] Zahn K, Méndez-Alcaraz J M and Maret G 1997 *Phys. Rev. Lett.* **79** 175

[138] Pesché R, Kollmann M and Nägele G 2002 *J. Chem. Phys.* **114** 8701
[139] Kollmann M, Hund R, Rinn B, Nägele G, Zahn K, König H, Maret G, Klein R and Dhont J K G 2002 *Europhys. Lett.* **58** 919
[140] Skjeltorp A T 1985 *J. Appl. Phys.* **57** 3285
[141] Skjeltorp A T 1995 *Physica* A **213** 30
[142] Martin J E, Anderson R A and Tigges C P 1998 *J. Chem. Phys.* **108** 3765
[143] Halsey T C and Toor W 1990 *Phys. Rev. Lett.* **65** 2820
[144] Toor W R 1993 *J. Colloid Interface Sci.* **156** 335
[145] Dassanayaka U, Fraden S and van Blaaderen A 2000 *J. Chem. Phys.* **112** 3851
[146] Martin J E, Anderson R A and Tigges C P 1999 *J. Chem. Phys.* **110** 4854
[147] Ivey M, Liu J, Zhu Y and Cutillas S 2000 *Phys. Rev.* E **63** 011403
[148] Liu J, Lawrence E M, Wu A, Ivey M L, Flores G A, Javier K, Bibette J and Richard J 1995 *Phys. Rev. Lett.* **74** 2828
[149] Flores G A, Liu J, Mohebi M and Jamasbi N 1999 *Phys. Rev.* E **59** 751
[150] Tao R and Sun J M 1991 *Phys. Rev. Lett.* **67** 398
[151] Halsey T C and Toor W 1990 *J. Stat. Phys.* **61** 1257
[152] Silva A S, Bond R, Plouraboué F and Wirtz D 1996 *Phys. Rev.* E **54** 5502
[153] Cutillas S and Liu J 2001 *Phys. Rev.* E **64** 011506
[154] Furst E M and Gast A P 2000 *Phys. Rev.* E **61** 6732
[155] Furst E M and Gast A P 2000 *Phys. Rev.* E **62** 6916
[156] Zhou L, Wen W and Sheng P 1998 *Phys. Rev. Lett.* **81** 1509
[157] Gross M and Kiskamp S 1997 *Phys. Rev. Lett.* **79** 2566
[158] Tao R and Sun J M 1991 *Phys. Rev.* A **44** R6181
[159] Friedberg R and Yu Y-K 1992 *Phys. Rev.* B **46** 6582
[160] Chen T, Zitter R N and Tao R 1992 *Phys. Rev. Lett.* **68** 2555
[161] Davis L C 1992 *Phys. Rev.* A **46** R719
[162] Gross M and Wei C 2000 *Phys. Rev.* E **61** 2099
[163] Schulz B and Baberschke K 1994 *Phys. Rev.* B **50** 13467
[164] Demand M, Padovani S, Hehn M, Ounadjela K and Bucher J P 2002 *J. Magn. Magn. Mater.* **247** 147
[165] Iglesias O and Labarta A 2000 *J. Magn. Magn. Mater.* **221** 149
[166] MacIsaac A B, Whitehead J P, De'Bell K and Poole P H 1996 *Phys. Rev. Lett.* **77** 739
[167] MacIsaac A B, De'Bell K and Whitehead J P 1998 *Phys. Rev. Lett.* **80** 616
[168] Taylor M B and Gyorffy B L 1993 *J. Phys.: Condens. Matter* **5** 4527
[169] Booth I, MacIsaac A B, Whitehead J P and De'Bell K 1995 *Phys. Rev. Lett.* **75** 950
[170] Vedmedenko E Y, Oepen H P, Ghazali A, Lévy J-C S and Kirschner J 2000 *Phys. Rev. Lett.* **84** 5884
[171] MacIsaac A B, Whitehead J P, Robinson M C and De'Bell K 1995 *Phys. Rev.* B **51** 16033
[172] Usadel K D and Hucht A 2002 *Phys. Rev.* B **66** 024419
[173] Wolff U 1989 *Phys. Rev. Lett.* **62** 361
[174] Creutz M 1992 *Phys. Rev. Lett.* **69** 1002
[175] Stoycheva A D and Singer S J 2000 *Phys. Rev. Lett.* **84** 4657
[176] Abu-Labdeh A M, Whitehead J P, De'Bell K and MacIsaac A B 1995 *Phys. Rev.* B **65** 024434
[177] Deng D S, Jin X F and Tao R 2002 *Phys. Rev.* B **65** 132406
[178] Russier V 2001 *J. Appl. Phys.* **89** 1287
[179] Siu Y L, Wan J T K and Yu K W 2001 *Phys. Rev.* E **64** 051506
[180] Yan Q and de Pablo J J 2000 *J. Chem. Phys.* **113** 1276
[181] Landau D P and Binder K 2000 *A Guide to Monte Carlo Simulations in Statistical Physics* (Cambridge: Cambridge University Press)
[182] Attard P, Kjellander R, Mitchell D J and Jönsson B 1988 *J. Chem. Phys.* **89** 1664
[183] Attard P and Patey G N 1991 *Phys. Rev.* A **43** 2953
[184] Moschel A and Usadel K D 1995 *Phys. Rev.* B **51** 16111
[185] Hucht A and Usadel K D 1997 *Phys. Rev.* B **55** 12309